Mechanics of Materials 17 (1994) 175–193
Elsevier

Evolution of microstructure and shear-band formation in α-hcp titanium

M.A. Meyers [a]*, G. Subhash [b], B.K. Kad [a], L. Prasad [a]

[a] *University of California, San Diego, La Jolla, CA 92093-0411, USA*
[b] *Michigan Technological University, Houghton, Michigan, USA*

Received 9 January 1993; revised version received 20 October 1993

The evolution of the microstructure generated by high strain-rate plastic deformation of titanium was investigated. A testing geometry generating controlled and prescribed plastic strains under an imposed stress state close to simple shear was used; this testing procedure used hat-shaped specimens in a compression Kolsky bar which constrains the plastic deformation to a narrow region with approximately 200 μm width. Within this band, localization sets in, initiated at geometrical stress concentration sites, at a shear strain of approximately 1.4. The shear-band widths vary from 3 to 20 μm and increase with plastic strain. High strain-rate deformation induces, at lower plastic strains ($\gamma < 1.4$), planar dislocation arrays and profuse twinning in titanium. In the vicinity of the shear band, elongated cells are formed, which gradually transform into sub-grains. The break-up of these sub-grains inside the band leads to a microstructure composed of small grains (~ 0.2 μm) with a relatively low dislocation density. The combined effects of plastic strain and temperature on the microstructural recovery processes (dynamic recovery and recrystallization) are discussed. The experimental results are compared with predictions using a phenomenological constitutive equation and parameters obtained from compression experiments conducted over a wide range of strain rates.

The experimental results indicate that the formation of shear bands occurs in two stages: (a) instability, produced by thermal softening and the enhancement of the thermal assistance in the motion of dislocations; (b) localization, which requires softening due to major microstructural changes (recovery and recrystallization) in the material. The calculated temperature rises required for instability and localization are 350 K and 776 K, respectively. Whereas instability may occur homogeneously throughout the entire specimen, localization is an initiation and propagation phenomenon, starting at geometrical (stress concentration sites) or microstructural inhomogeneities and propagating as a thin (3–20 μm) band.

1. Introduction

The evolution of the microstructure in high-strain, high strain-rate deformation has recently been the object of considerable attention; it is of particular importance within shear instabilities (bands) generated at high strain rates, because of the significant thermal excursions involved in the process. These thermal excursions, enabled by the adiabatic or quasi-adiabatic conditions, coupled with high plastic strains (shear strains as high as 570 have been reported (Moss, 1981) create a thermo-mechanical environment that is unique and profoundly affects the microstructure within the shear localization region. The research reported herein represents the result of an effort aimed at characterizing the evolution of this microstructure in a material well known for its propensity to form adiabatic shear bands. The characterization of the microstructure and development of a mechanistic understanding of the processes involved are necessary prerequisites for obtaining physically-based constitutive equations that describe the process and have a predictive capability.

The formation of a shear band has as a necessary condition the instability in the stress–strain

* Corresponding author.

SSDI 0167-6636(93)E0089-K

response under the imposed conditions, i.e., $d\tau/d\gamma \leqslant 0$. This instability criterion has been used by Recht (1964) and Culver (1973) in the prediction of a plastic (homogeneous) strain at which the shear band initiates. It has been found experimentally and analytically that this condition is not sufficient and that perturbations are necessary for the onset of shear localization. This perturbation analysis has been introduced independently by Bai (1981) and Clifton (1981) and has been further developed and extensively used by Fressengeas and Molinari (1987) and Wright (1987; 1989). Culver (1973) and Bai (1981) calculated instability strains for titanium. Duffy and co-workers (Hartley et al., 1987; Marchand and Duffy, 1988) developed and experimental technique to measure strains, strain rates, and temperatures within a shear band and were able to distinguish the sequential stages of instability and localization in the stress–strain curve due to shear-band formation. Their temperature evolution measurements within shear bands are classic experiments of a pioneering nature. The dedication of this volume to Professor Duffy is a tribute by researchers in the field to his contributions.

Early microstructural studies within the shear bands in titanium have been limited to optical microscopy, which cannot reveal the distinguishing features within the bands. In 1985, Grebe et al. (1985) identified a microcrystalline structure in titanium; subsequent detailed transmission electron microscopy by Meyers and Pak (1986) revealed that the shear band consisted of small grains with sizes ranging between 0.05 and 0.3 μm; calculations suggested that this structure was formed during, and not after, plastic deformation. Independent work by Stelly and Dormeval (1986) confirmed the nature of the microstructure within the shear band. Timothy and Hutchings (1985), Timothy (1987), and Winter (1975) also discuss shear-band formation in titanium alloys.

The experiments described herein had as objectives: (a) the controlled generation of shear bands at prescribed strains and strain rates; (b) the determination of instability and localization strains; and (c) the characterization of the microstructural evolution leading to the final, microcrystalline structure.

2. Experimental techniques

Commercial purity titanium (Grade 2, with the following contents (wt%) of impurities: C (0.03), O_2 (0.122), H_2 (0.0051), N_2 (0.014)) in the annealed condition (750°C for 2 h and air cooled) was chosen as the material for this study. The grains were equiaxed and the grain size, as measured by the mean linear intercept, was equal to 72 μm. The material was obtained in the form of 1 in (25.4 mm)-thick bar. Two types of specimens were machined from the bar: conventional cylindrical specimens (6.25 mm diameter and lengths of 5 and 6.25 mm for dynamic and quasi-static tests, respectively), prepared by electrical discharge machining, and hat-shaped specimens, for controlled shear-band experiments. The axes of cylindrical and hat-shaped specimens were parallel to the lingitudinal axis of the stock bar. Fig. 1a shows the overall configuration of the hat-shaped specimen; this morphology and testing procedure were developed by Hartmann et al. (1981) and Meyer and Manwarig (1986) and used recently by Beatty et al. (1992) for AISI 4340 steel and Meyers et al. (1992) for copper. The specimen is placed between the incident and transmitter bars in a Hopkinson (Kolsky) bar and a spacer ring ensures a prescribed displacement in the principal plastic deformation area indicated in Fig. 1. The stress state in the plastic deformation region is fairly close to simple shear and the plastic strain is approximately equal to the ratio between the shear displacement d (Fig. 1a) and the thickness of the plastic deformation region, t (Fig. 1b); the shear stress is equal to the load, P, divided by the area of the resisting region

$$\tau \simeq P\left[\pi h\left(\frac{d_i + d_e}{2}\right)\right], \tag{1}$$

where d_i is the internal and d_e is the external diameter, and h is the height of the area (Fig. 1a). Fig. 1b shows the region of concentrated shear deformation. Subsequent to mechanical testing, the hat-shaped specimens were sectioned longitudinally for observation by optical microscope.

The samples were polished and etched in a

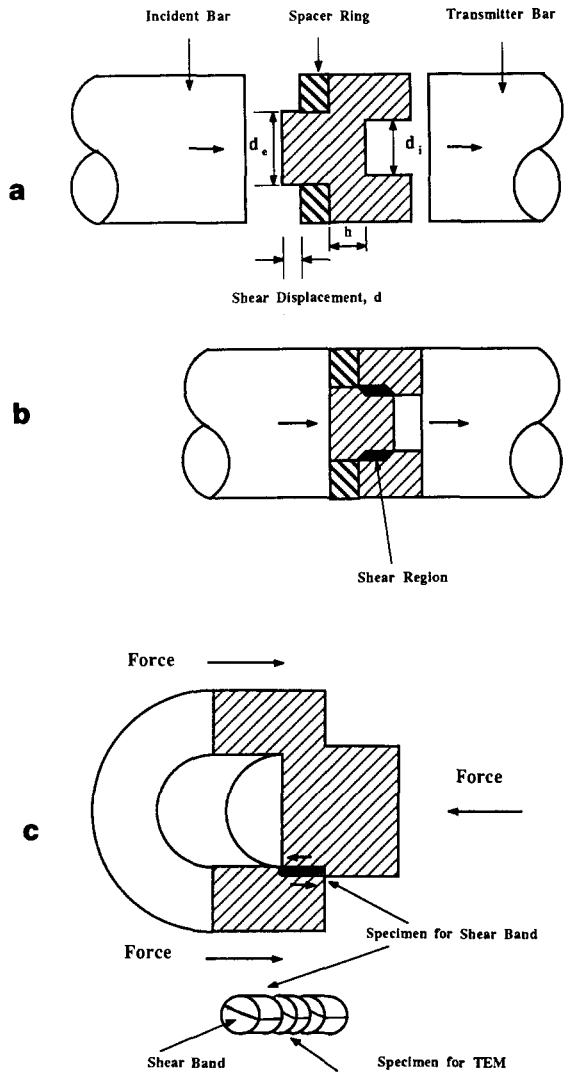

Fig. 1. (a) Longitudinal section of hat-shaped specimen, stopper ring, and testing configuration in Hopkinson bar; (b) specimen after testing with concentrated shear region; (c) extraction of specimen for transmission electron microscopy.

solution of 5% HF, 20% HNO_3 and 75% H_2O for optical microscopy. Specimens for electron microscopy were obtained by cutting, by electrical discharge machining, cylinders with 3 mm diameter oriented as shown in Fig. 1c. These cylinders were then sectioned into disks (1 mm thick), with the central region used for electron microscopy. The disks were hand-ground to 0.2 mm and electropolished in an HF, H_2SO_4, and methanol solution of -40°C. Perforation tended to occur preferentially on the shear band. TEM foils were examined in a Philips C-M30 electron microscope operating at 100, 200 and 300 kV.

3. Results and discussion

3.1. Mechanical testing

Mechanical tests were conducted on cylindrical specimens at strain rates between 2×10^{-4} s^{-1} and 3.9 s^{-1} in an MTS servohydraulic machine, and at strain rates between 9×10^{2} s^{-1} and 7.6×10^{3} s^{-1} in a compression Hopkinson (Kolsky) bar. The result of these experiments are

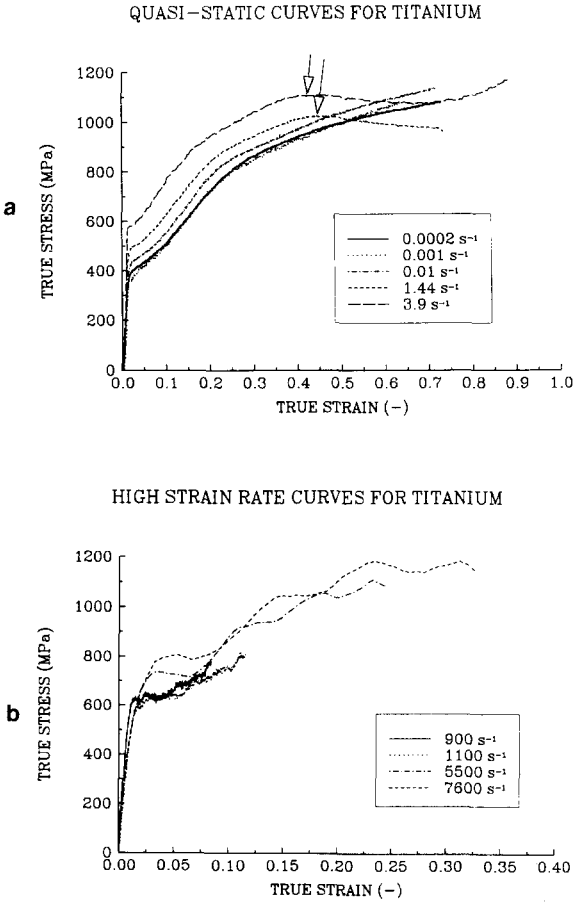

Fig. 2. (a) Quasi-static; and (b) dynamic response of cylindrical titanium specimens at ambient temperatures.

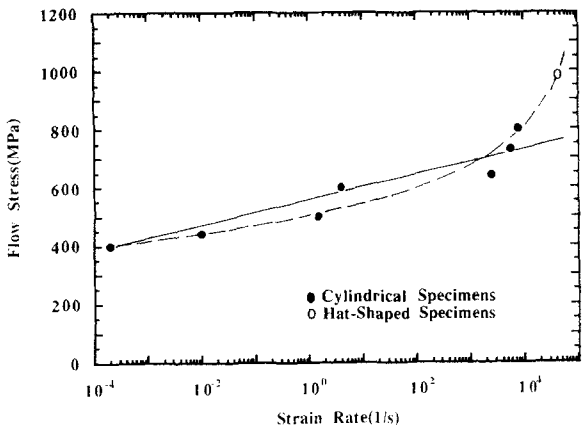

Fig. 3. Flow stress (at 1pct plastic strain) as a function of strain rate for cylindrical titanium specimens.

shown in Figs. 2a and 2b, respectively. The material clearly exhibits a strain-rate sensitivity as shown in the plot of Fig. 3, where the flow stress at 1 pct plastic strain is plotted against the logarithm of the strain rate. There seems to be an increase in the slope at the high strain-rate end of the spectrum; nevertheless, for simplicity a linear least squares fit was made. Titanium has a low thermal conductivity, and the strain rate at which heat extraction from the specimens ceases to be sufficient for isothermal behavior can be calculated fairly expediently. The specimen size, L, which ensures isothermal behavior is

$$L \simeq 2\sqrt{\alpha t}\,, \tag{2}$$

where α is the thermal diffusivity (equal to the ratio $K/\rho C$, where K, ρ, and C are the thermal conductivity, density, and heat capacity, respectively) and t is the duration of the test. This is discussed in greater detail in Section 3.3, where it is established that thermal effects become important at $\dot{\epsilon} \simeq 1\ s^{-1}$. Observations in Fig. 2a confirm that instability is observed at this strain rate; the curve exhibits a maximum at $\epsilon \sim 0.45$ (see arrows). The dynamic tests on hat-shaped specimens were conducted to different total displacements, d. Table 1 shows the prescribed displacements for the different tests conducted. They varied from 0.28 to 1.5 mm. A typical stress–displacement response, as obtained from the Kolsky

Table 1
Prescribed displacements, d, and shear-band widths, for hat-shaped specimens

Specimen	Displacement, d (mm)	Band thickness (μm)
A	0.28	2.6
B	0.41	3.7
C	0.43	7.1
D	0.46	8.6
E	0.51	14.4
F	0.56	13.7
G	0.58	16.2
H	0.64	7.4
I	0.68	9.8
J	1.5	18.9

bar experiment, is shown in Fig. 4. The onset of localization (shear-band formation) is clearly evident from the drop in the shear stress–displacement curve. This drop in stress occurs at a displacement, d, of ~ 0.4 mm (see arrow). The shear strength of the material decreases from ~ 500 MPa to 100–200 MPa. The first two fluctuations are due to wave-propagation and machine–specimen interactions. The plot of Fig. 4 represents the response of specimen J, with a total maximum prescribed displacement of 1.5 mm. The stress rise on the right-hand side of Fig. 4 corresponds approximately to this displacement. This test, conducted to a maximum displacement, enabled a series of experiments (designated A–J in Table 1) in which the onset of localization could be bracketed with reasonable accuracy. The average strain rate in the hat-shaped specimens is calculated from the velocity

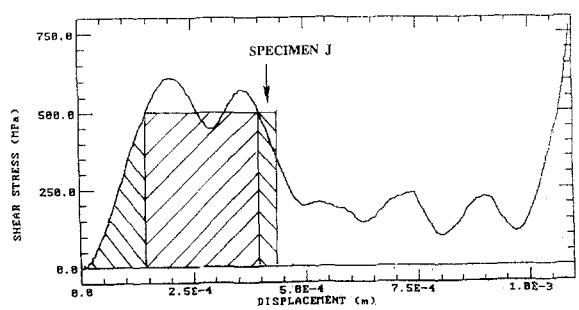

Fig. 4. Shear stress versus displacement (plot for hat-shaped specimen (specimen J in Table 1).

of the incident bar, v, divided by the thickness of the plastic deformation region, t:

$$\dot{\gamma} = v/t.$$

The thickness of the plastic deformation region, as will be reported in Secton 3.2, was measured from optical micrographs of recovered specimens and is equal to ~ 200 μm. This region is approximately twice the difference $(d_e - d_i)/2$, shown in Fig. 1a. The specimen dimensions were:

$d_e = 10.15$ mm,

$d_i = 9.98$ mm,

$$\frac{d_e - d_i}{2} \simeq 0.09 \text{ mm} = 90 \text{ μm}.$$

For a bar velocity of 8 m/s, one obtains

$$\dot{\gamma} = \tfrac{8}{0.2} \times 10^3 = 4 \times 10^4 \text{ s}^{-1}.$$

The maximum average shear stress in the plastically-deformed region of the hat-shaped specimens can be converted into a uniaxial stress through:

$$\tau_{max} = \frac{\sigma}{2}.$$

Fig. 4 yields (the mid-point of the Pochhammer–Chree oscillations was taken as the stress value):

$\tau_{max} \simeq 500$ MPa.

Thus:

$\sigma \simeq 1{,}000$ MPa.

The average shear strength of specimens A–J (Table 1) was 490 MPa, consistently with specimen J (shown in Fig. 4); this yields $\sigma = 980$ MPa. The highest yield stress for the cylindrical tests was 800 MPa. This higher shear strength seems to be indicative of a change in slope from the linear one (full line) towards a more pronounced line (dashed line) on Fig. 3. The average strength of the hat-shaped specimens is shown in Fig. 3 (symbol ○). This aspect will be discussed further in Section 3.3.

3.2. Characterization

The hat-shaped specimens were sectioned as shown in Fig. 1c and characterized optically and by transmission electron microscopy. Low-magnification optical micrographs of the shear localization region are shown in Fig. 5. The onset of shear localization occurs at a shear displacement of ~ 0.4 mm, in accordance with the results shown in Fig. 4. Profuse mechanical twinning is observed in the shear deformation region, together with the bending of the grains. At a displacement of 0.406 mm the notches at the ends of the shear deformation region show the onset of localization (seen in greater detail in Fig. 7). At a displacement $d = 0.432$ mm the shear band is fully formed. There is a tendency towards an increase in the shear-band width with displacement, as can be seen by comparing the shear in Fig. 5. These widths were measured and are plotted in Fig. 6. The widths tend to saturate at 20 μm. The strain marked in the abscissa of Fig. 6 is the plastic shear strain obtained by dividing the displacement d by the width of the homogeneous deformation region (~ 0.2 mm). This measured width is compared with the value predicted using the equation proposed by Bai; the half-width of the shear band, δ, was proposed by Bai et al. (1986); Dodd and Bai (1989); Bai (1990) to be equal to:

$$\delta \simeq (\lambda/T\tau\dot{\gamma})^{1/2}. \tag{3}$$

By inserting the parameters:

$\tau = 490$ MPa,

$\dot{\gamma} = 5 \times 10^4 \text{ s}^{-1}$,

$T = 975\ K (= T_m/2)$,

$\lambda = 22.4\ J \text{ s}^{-1} \text{ m}^{-1} \text{ K}^{-1}$,

one obtains $\delta \simeq 30$ μm, which corresponds to a thickness of 60 μm. This three-fold difference between experimentally observed and calculated results is due to uncertainties in τ, $\dot{\gamma}$, and T. Nevertheless, the results can be considered to be in fair accord.

The microhardnesses of the shear bands ($\approx$ 200–220 VHN) were not significantly higher than the adjoining matrix ($\approx$ 160–200 VHN). This factor is easily explainable after the microstructure was characterized by transmission electron microscopy.

Optical micrographs at higher magnification are shown in Figs. 7 and 8. Fig. 7c shows the

concentrated plastic deformation region (specimen A) prior to the initiation of localization. The thickness of this region is approximately 200 μm. The onset of localization occurred at the corners of the hat-shaped specimen; these are stress-concentration sites. Fig. 7b (specimen B) shows this onset on the left-hand side; ahead of the tip of the band a region with intense plastic deformation is formed. In Fig. 7c the tip of the band (B) and the region of intense plastic deformation are very visible. The thickness of the plastic deformation region is reduced to its initial value of 200 μm. Fig. 8 shows the shear bands at higher imposed displacements: (a) 0.46 (specimen D); (b) 1.5 mm (specimen J); and (c) 1.5 mm (edge of specimen J). The shear band is clearly defined and the microstructure inside of the band cannot be revealed by optical microscopy, because of its fine scale. The bending undergone by deformation twins (marked by arrow) is extreme, and the shear strain at the boundary is ~ 5 (see triangle). As the applied displacement, d, increases, the thickness of the band also increases, reaching the final value shown in Fig. 8b. The small irregularities seen on the surface of the band are caused by the micrograins. At large imposed shear strains,

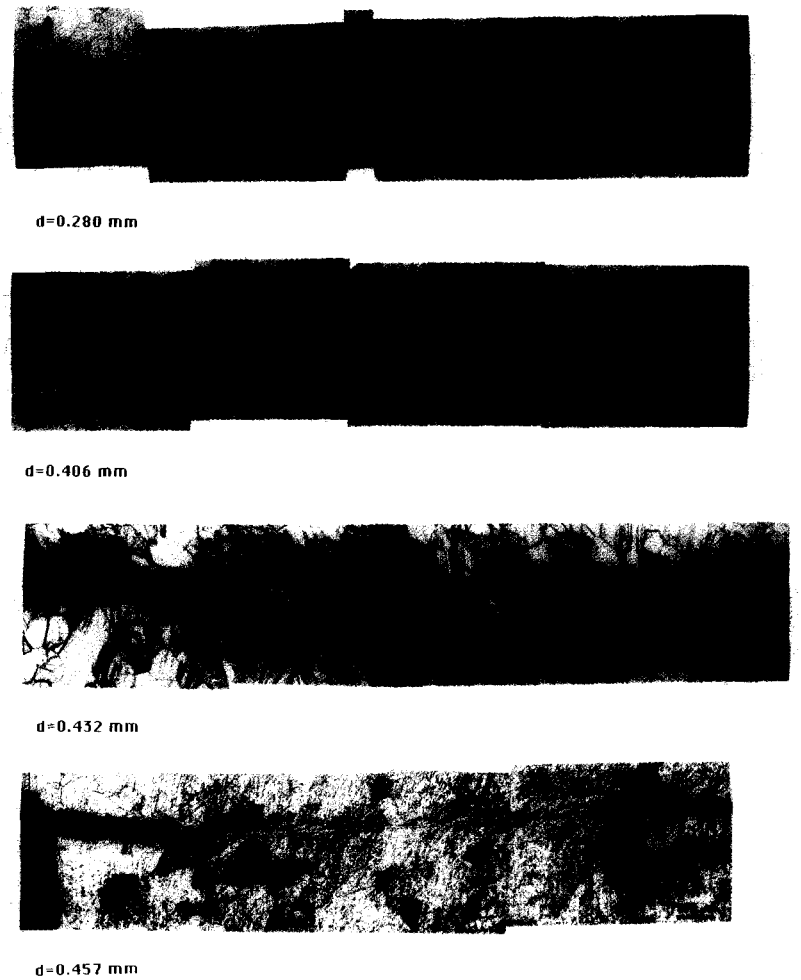

Fig. 5. Formation of plastic deformation region and shear band at shear region in hat-shaped specimen; shear displacements imposed shown for each condition (specimens A through J in Table 1).

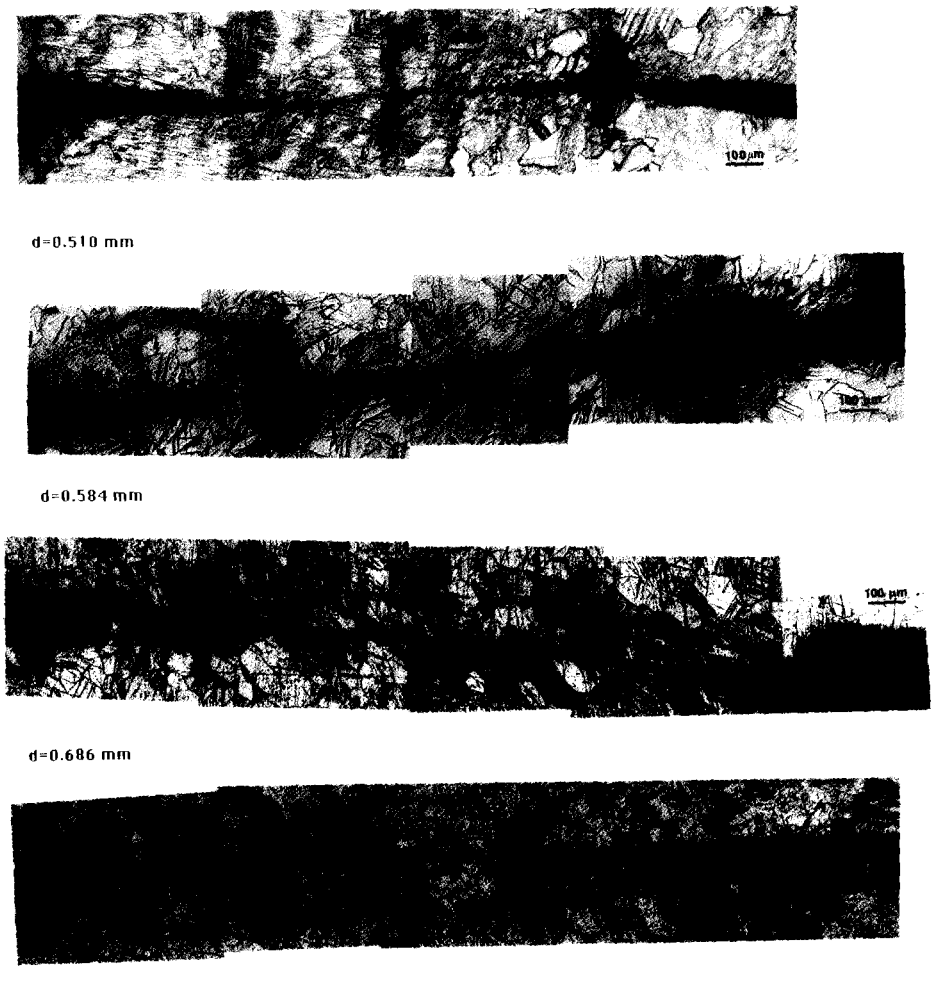

Fig. 5 (continued).

the shear band is a preferred path for crack propagation, as shown in Fig. 8c; this propensity for crack propagation along shear bands is well known (e.g., Grebe et al., 1985).

Transmission electron microscopy was conducted on specimens taken from three conditions representative of the entire spectrum of displacements shown in Table 1: specimens B (no shear band), D (early formation of shear band) and J ("mature" shear band) were characterized and the microstructures are shown in Figs. 10–16. Prior to shear-band formation the specimen undergoes a high strain-rate plastic deformation, yielding considerable deformation twinning (easily visible in Figs. 5, 7, and 8). Consistently with the propensity for mechanical twinning, dislocation arrays tended to be planar. These parallel arrays of dislocations are shown in Fig. 10. The edge components of dislocations have a higher mobility and advance (loops marked A) leaving behind screw components as straight lines. Fig. 10b shows a higher magnification of these arrays: in some instances dislocation dipoles seem prominent, although no effort was made to identify them. The grouping of dislocations into bands is seen very clearly in Fig. 11a with a mean spacing between

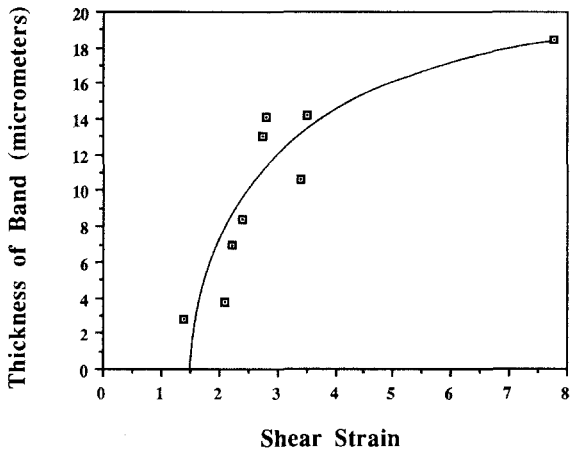

Fig. 6. Thickness of shear bands as a function of imposed shear displacement.

parallel slip bands as ≈ 1–1.5 μm. In a majority of the cases, a single slip system dominates in a grain which explains the planar arrays. However, in some instances multiple slip was activated on intersecting planes. Such intersecting slip bands leave considerable sessile debris as shown in Fig. 11b. Fig. 11b shows one such intersection site between two bands.

At the high displacement end of the spectrum ($d = 1.5$ mm, specimen J) the shear band is well formed and the microstructure is radically different. The material close to the shear band exhibited a high density of dislocations, arranged in elongated cells (Fig.12a). Fig. 12b shows the break-up of these elongated cells, at the boundary of the shear band. Since the observation was made on a plane perpendicular to the shear direction, the tri-dimensional shape of the elongated cells is expected to be a prolate spheroid ("pancake"). The cell walls are clearly delineated in Fig. 12b; these cells break up into grains and subgrains. Fig. 13 shows two micrograins in the middle of the shear band in specimen J. These micrograins have diameters of ~ 0.2 μm, a low dislocation density, and grain boundaries which are free of defects.

In specimen D (shear displacement of 0.46 mm) similar features were observed: elongated subgrains and equiaxed micro- (or sub-) grains. Fig. 14 shows a mixture of these features. Addi-

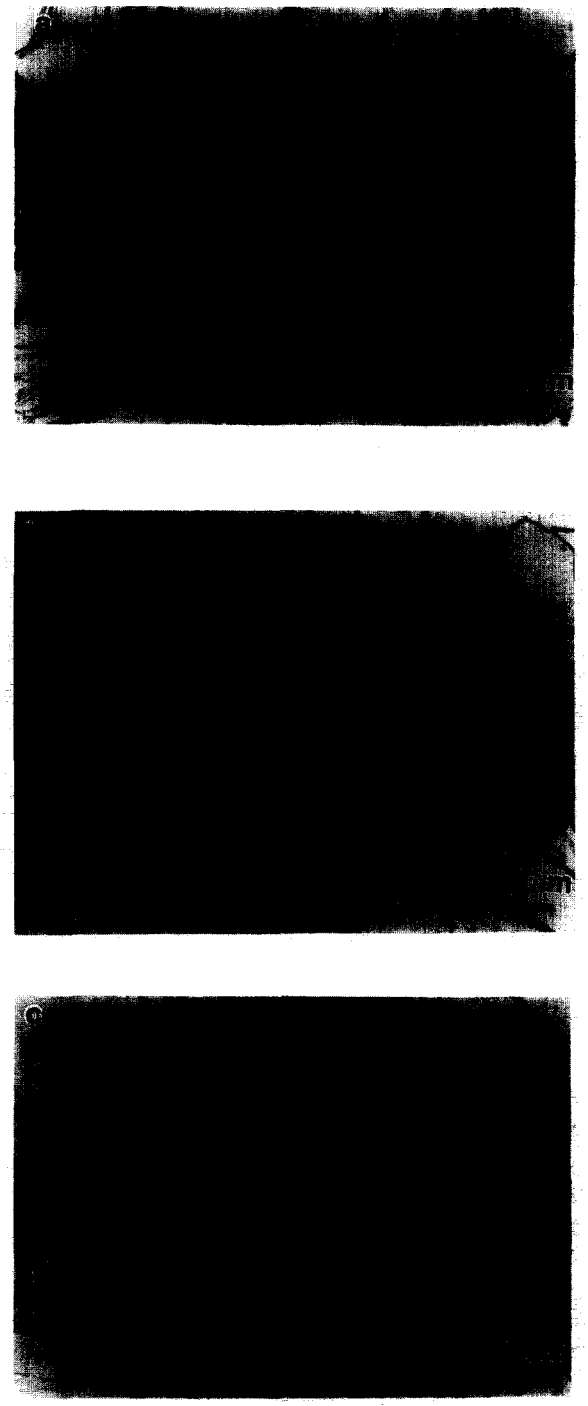

Fig. 7. Optical micrographs of shear deformation regions in hat-shaped specimens: (a) prior to shear-band initiation; (b) at onset (left-hand side) of shear-band formation; (c) early shear band and shear-band tip.

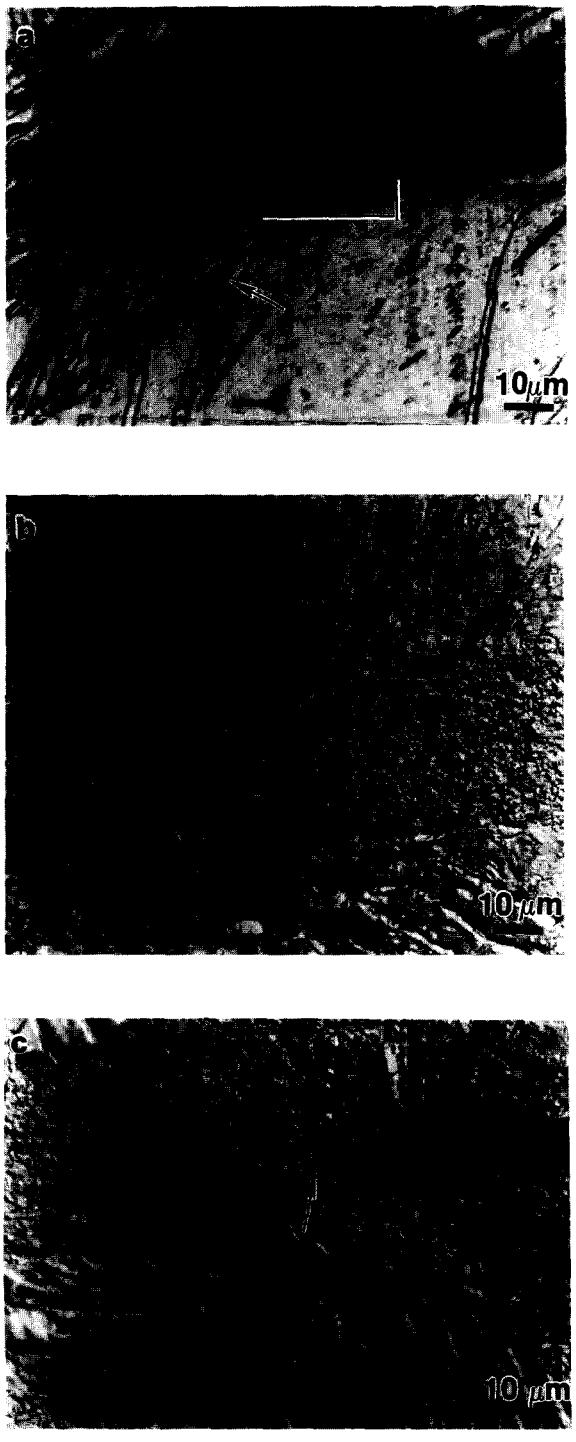

Fig. 8. Optical micrograph of well developed shear bands at increasing shear displacements: (a) specimen D; (b) specimen J; (c) edge of specimen J.

tional micrograins in specimen D are shown in Figs. 15 and 16. One encounters regions with high and low dislocation densities; this is indicative of an on-going recrystallization process in which recently formed micrograins (free of dislocations) are adjacent to heavily deformed materials. The electron micrographs shown in Figs. 10–16 indicate that the following sequence of plastic deformation takes place in the shear deformation region: (a) planar dislocation arrays and deformation twins; (b) elongated cells; (c) elongated subgrains; (d) break-up of subgrains into equiaxed micrograins.

The hardness results shown in Fig. 9 can also be rationalized in terms of the deformation structure. The material adjacent to the band is work hardened by dislocations and deformation twins; inside the shear band, the strength increase comes from a reduction in grain size. The two effects lead to similar hardnesses.

The exact nature of the break-up process is not fully understood at present. Derby (1992) recently conducted a systematic analysis of dynamic recrystallization and considered two mechanisms: nucleation and growth of recrystallized grains in a deformed material (classical recrystallization) and formation of recrystallization by the gradual rotation of subgrains (rotation recrystallization). These dynamic recrystallization mechanisms are shown in Fig. 17 in a schematic fashion. Both mechanisms lead to the break-up of the original grain structure. In classical (or migration) recrystallization (Fig. 17a) new grains are nucleated at regions of high plastic strain, growing into the deformed material. In rotation recrystallization (Fig. 17b) the rotation of the cells and subgrains occurs gradually, until the dislocations are absorbed by the grain boundaries. Derby (1992) compared the Sandstrom–Lagneborg (1975) and Derby–Ashby (1987) analyses, and concluded that they lead to similar relationships between the imposed strain rate and the recrystallized grain size, λ;

$$\lambda = \frac{k}{\dot{\epsilon}^{1/2}},$$

where k is a parameter that incorporates a num-

ber of constants of either the Sandstrom–Lagneborg (1975) or Derby–Ashby (1987) theories. Although the analysis conducted by Derby (1992) applies to classical recrystallization and the microstructural evolution path shown in Figs. 12–16 shows elements of both classical (nucleation and growth) and rotation recrystallization, a comparison of the results was made. Derby (1992) proposes generalized relationships between grain (in dynamic recrystallization) and subgrain (in dynamic recovery) sizes and the applied stress. His results are shown in Fig. 18; a wide range of materials (ice, ceramics, rocks, metals) was used in determining their dynamic recovery and recrys-

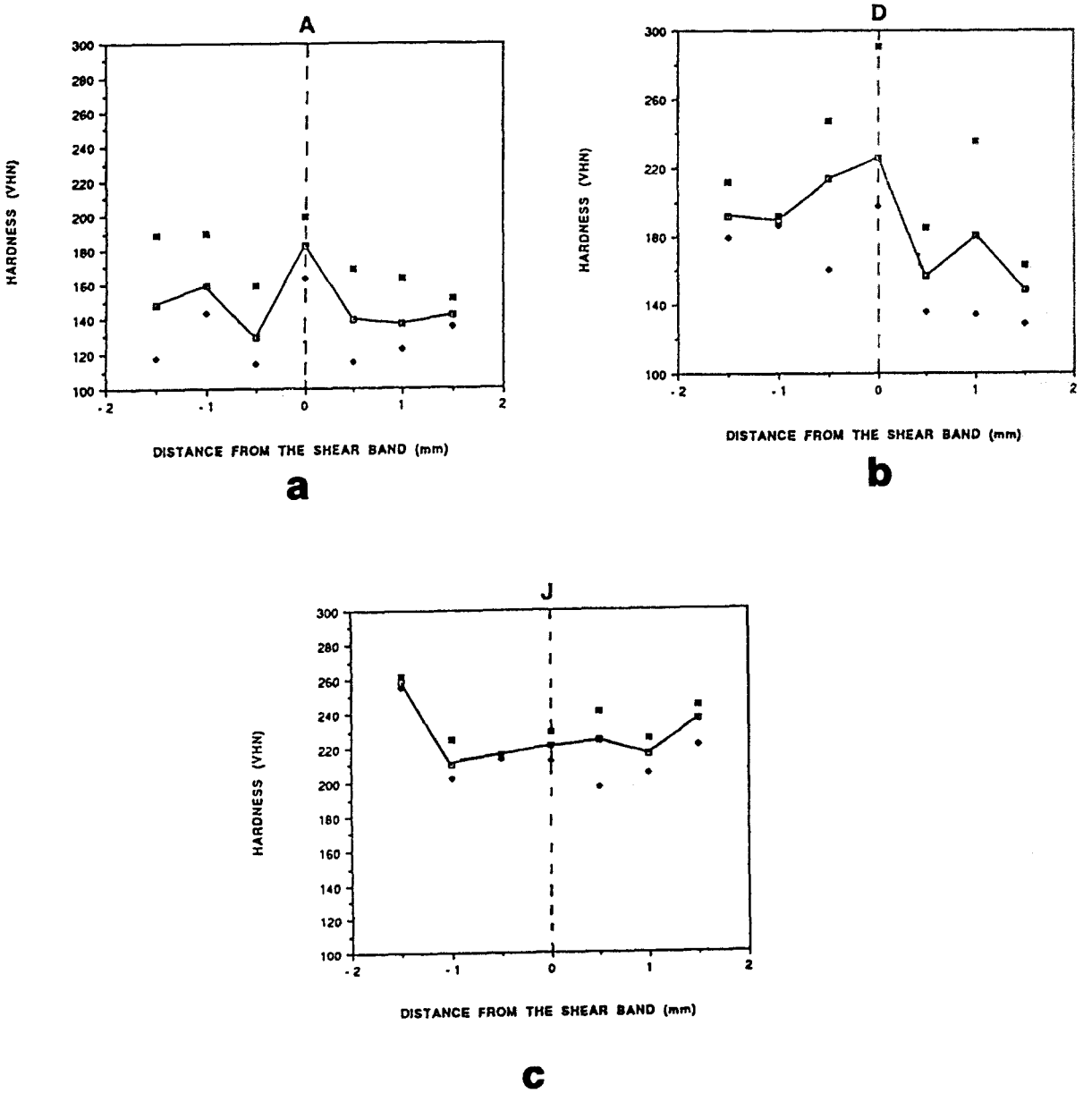

Fig. 9. Microhardnesses of shear bands for three specimens.

tallization bands. The results obtained in this investigation (grain or subgrain size of 0.2 μm at an imposed strain rate of 4×10^4 s^{-1}) are shown in the same plot; it is clear that they are consistent with either a dynamic recrystallization or recovery mechanisms, since the two responses converge. The results obtained for titanium are also consistent with the well known (e.g., Bird et al., 1969) relationship between normalized ap-

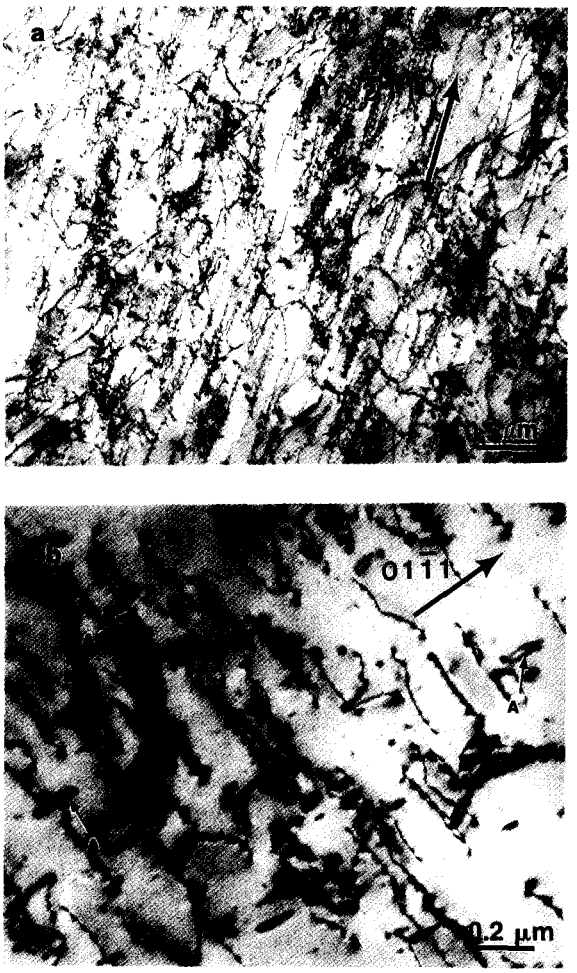

Fig. 10. Transmission electron micrograph of deformation substructure in shear deformation zone of hat-shaped specimen at displacement of 0.41 mm, prior to onset of shear band (specimen B): (a) profuse arrays of dislocations; (b) closer view of dislocations showing dipoles (marked by arrows).

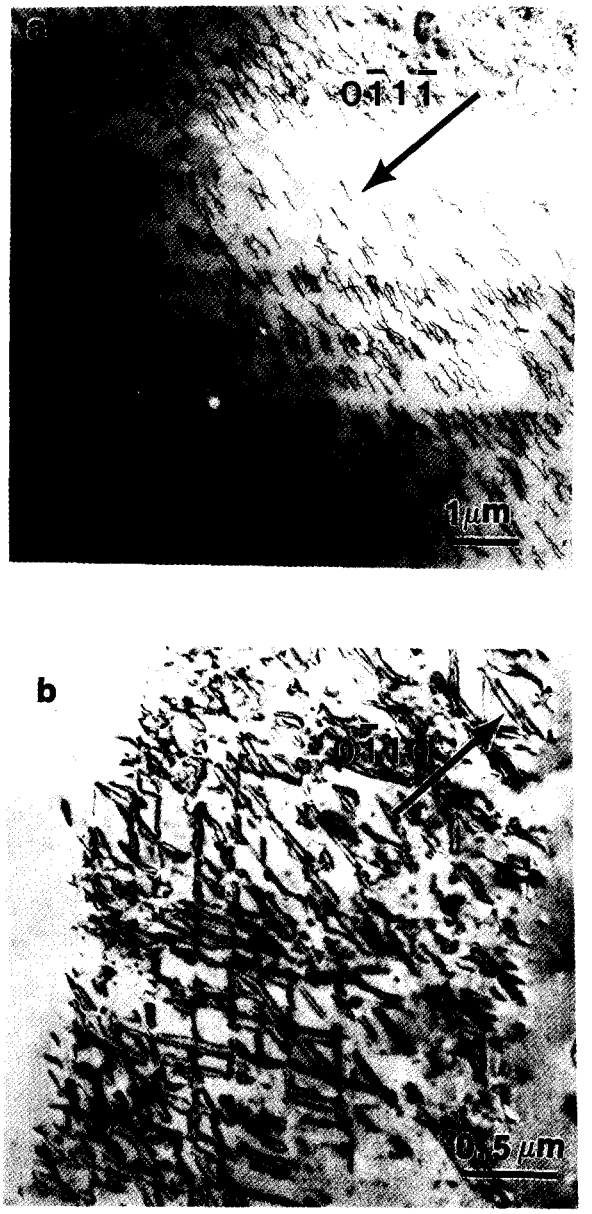

Fig. 11. TEM of specimen B (shear displacement at 0.41 mm): (a) linear dislocation arrays grouped in bands; (b) intersection of two bands.

plied stress and grain/subgrain size, λ:

$$\left(\frac{\sigma}{\mu}\right)\left(\frac{\lambda}{b}\right) \approx 20,$$

where μ and b are the shear modulus and Burg-

ers vector, respectively. At the high strain rates imparted in the hat-shaped specimens, $\sigma \simeq 1$ GPa. Thus:

$$\frac{1}{45}\frac{0.2\times10^{-6}}{0.3\times10^{-9}} = 10^3 = 15.$$

Thus, the microcrystalline structure observed within the shear band in titanium is consistent with dynamic recrystallization and/or recovery processes.

Fig. 12. TEMs of specimen J (shear displacement of 1.5 mm): (a) region adjoining shear band; (b) shear-band/adjoining region boundary.

3.3. Thermal analysis and constitutive modeling

The temperature evolution inside the specimen tested quasi-statically can be modelled by a one-dimensional heat conduction problem solved by Carslaw and Jaeger (1959). The specimen (length L) was compressed between steel platens. The heat conductivity of steel is fairly close to that of titanium, and, if one neglects convection losses to the air, the problem can be treated as a linear flow of heat in a solid in which heat is generated at a constant rate. Heat is generated in the region $x \pm L/2$, where L is the specimen length, and is extracted by the surroundings. The transition between the adiabatic and isothermal regimes can be calculated from the procedure described by Carslaw and Jaeger (1959) and corresponds to a temperature rise in the center of specimen of approximately 50 pct of the adiabatic temperature rise. Thus

$$L \simeq 2\sqrt{\alpha t},$$

where α is the thermal diffusivity and t is the duration of the test. One can define a critical strain rate by:

$$\dot{\epsilon}_{cr} = 4\alpha\epsilon/L^2.$$

For the quasi-static cylindrical specimens used in this investigation, $L_0 = 6.25$ mm. The critical strain rate obtained from the equation above is $\dot{\epsilon}_{cr} \simeq 1\ s^{-1}$. This predicted critical strain rate is fairly consistent with the results of Fig. 2a; both tests conducted at $1.44\ s^{-1}$ and $3.9\ s^{-1}$ show maxima in the stress–strain curves (marked by arrows A and B, respectively), whereas the tests conducted at lower strain rates exhibit continued work hardening. These maxima occur at $\epsilon \sim 0.45$.

The instability strain and temperature can be calculated by means of a constitutive equation that describes the response of the material as a function of strain, strain rate, and temperature:

$$\sigma = f(\epsilon, \dot{\epsilon}, T).$$

Numerous constitutive equations have been proposed; they are usually classified into phenomenological and physically-based models. The Johnson–Cook (1983) is the most common phe-

nomenological constitutive equation, whereas the MTS (Follansbee and Kocks, 1988), Zerilli and Armstrong (1987), and Klepaczo (1988) are the best known physically-based models. In this work a modified form the Johnson–Cook constitutive model with a power-law thermal softening term was applied to the experimental results in order to predict the instability strain and temperature. The following equation was used:

$$\sigma = (\sigma_0 + B\epsilon^n)\left(1 + C \log\frac{\dot{\epsilon}}{\dot{\epsilon}_0}\right)\left(\frac{T}{T_r}\right)^{\lambda}, \tag{4}$$

where σ_0, B, n, C, and λ are parameters determined experimentally; T and T_r are the current and reference (initial; 298 K) temperatures, respectively; $\dot{\epsilon}_0$ is the reference strain rate; σ and ϵ are the stress and strain, respectively.

The work of deformation can be incorporated into an (adiabatic) temperature rise,

$$dT = \frac{0.9}{\rho C_p}\sigma\, d\epsilon. \tag{5}$$

One arrives at a relationship between the temperature and plastic strain, at a fixed strain rate, by substituting Eq. (5) into Eq. (4):

$$T = \left[T_r^{-\lambda+1} + \frac{(1 + C \ln \dot{\epsilon}/\dot{\epsilon}_0)}{\rho C_p T_r^{\lambda}} \times 0.9(1-\lambda)\epsilon\left(\sigma_0 + \frac{B\epsilon^n}{n+1}\right)\right]^{1/1-\lambda}. \tag{6}$$

The instability strain can likewise be obtained by setting:

$$d\sigma/d\epsilon = 0. \tag{7}$$

This leads to:

$$\lambda(\sigma_0 + B\epsilon^n)^2 = -Bn\epsilon^{n-1}\frac{\rho C_p T_r^{\lambda}}{0.9} \times\left[T_r^{1-\lambda} + \frac{0.9\epsilon(1-\lambda)}{\rho C_p T_r^{\lambda}}\left(\sigma_0 + \frac{B\epsilon^n}{n+1}\right)\right]. \tag{8}$$

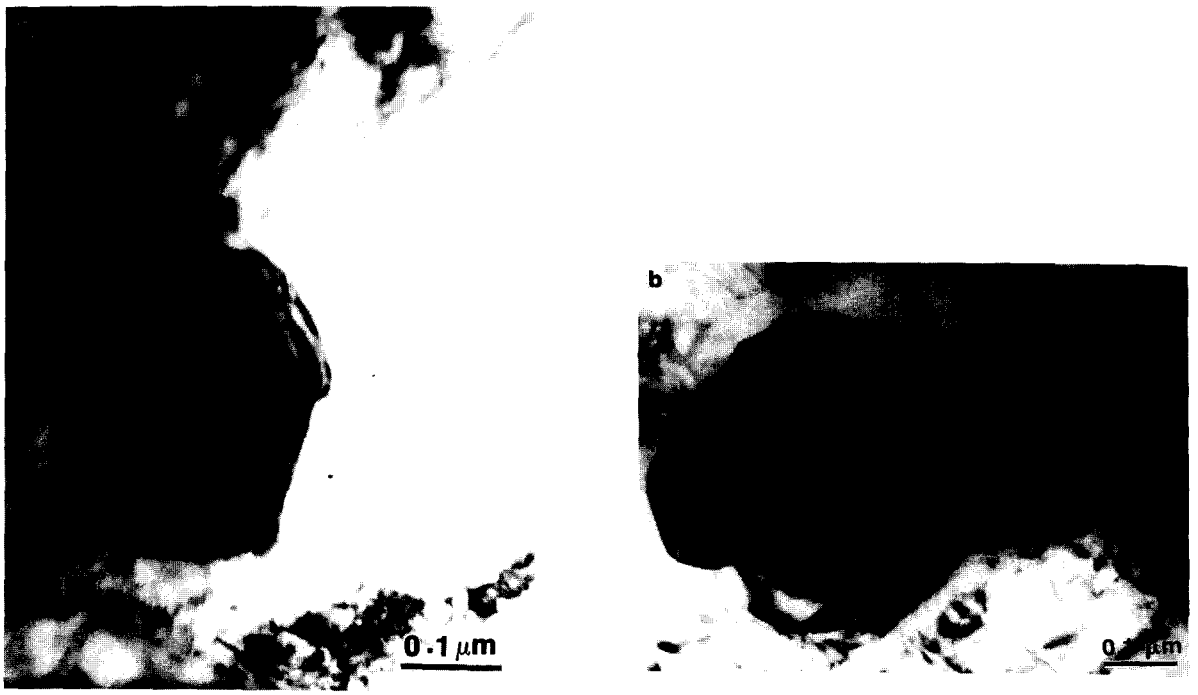

Fig. 13. (a, b) Micrograins within shear band in specimen J (shear displacement of 1.3 μm); notice low dislocations density within grains.

The parameters σ_0, B, n, C, and λ were determined from the experimental results displayed in Fig. 2. The reference strain rate $\dot{\epsilon}_0$ was taken as 10^{-2} s^{-1}, because the stress–strain curve does not exhibit any thermal softening. The logarithmic plot yields the slope, $n = 0.4$, and the intercept, $B = 940$ MPa. It should be noticed that this is an approximation and that the stress–strain curves shown in Fig. 2 display considerable deviation from this simple power function. The initial value of σ_0 is taken in such a manner that the experimental results match the predictions at higher strains ($\sigma_0 = 320$ MPa).

The strain-rate sensitivity, C, is obtained from Fig. 3, assuming a linear behavior (full line). The following value was obtained: $C = 0.1$. The thermal softening parameter, λ, was obtained experimentally by carrying out low strain-rate tests at varying temperatures and by fitting the flow stress, at a plastic strain of 0.1, into a power function. Fig. 19a shows the complete stress–strain curves at various temperatures, whereas Fig. 19b shows the power-law fit to the flow stresses. This power law relation does not apply to temperatures greater than the melting point (1940 K) because it does not predict a flow stress equal to zero; nevertheless, the flow stress is fairly close to zero (20 MPa).

The use of Eq. (6) enables the calculation of the temperature as a function of plastic strain for material; this is shown in Fig. 20, at two strain rates: 10^{-2} and 10^{4} s^{-1}. Instability strains and temperatures can be calculated by Eq. (8). The results are:

10^{-2} s^{-1}: $\epsilon_i = 0.2$, $T_i = 347$ K,

10^{4} s^{-1}: $\epsilon_i = 0.1$, $T_i = 344$ K.

These values are lower than the maxima in the stress–strain curves observed in Fig. 2a and marked by arrows. The reasons are: (a) that the flow stress shows a more complex temperature dependence, and drops less at temperatures close to ambient; and (b) that heat extraction from

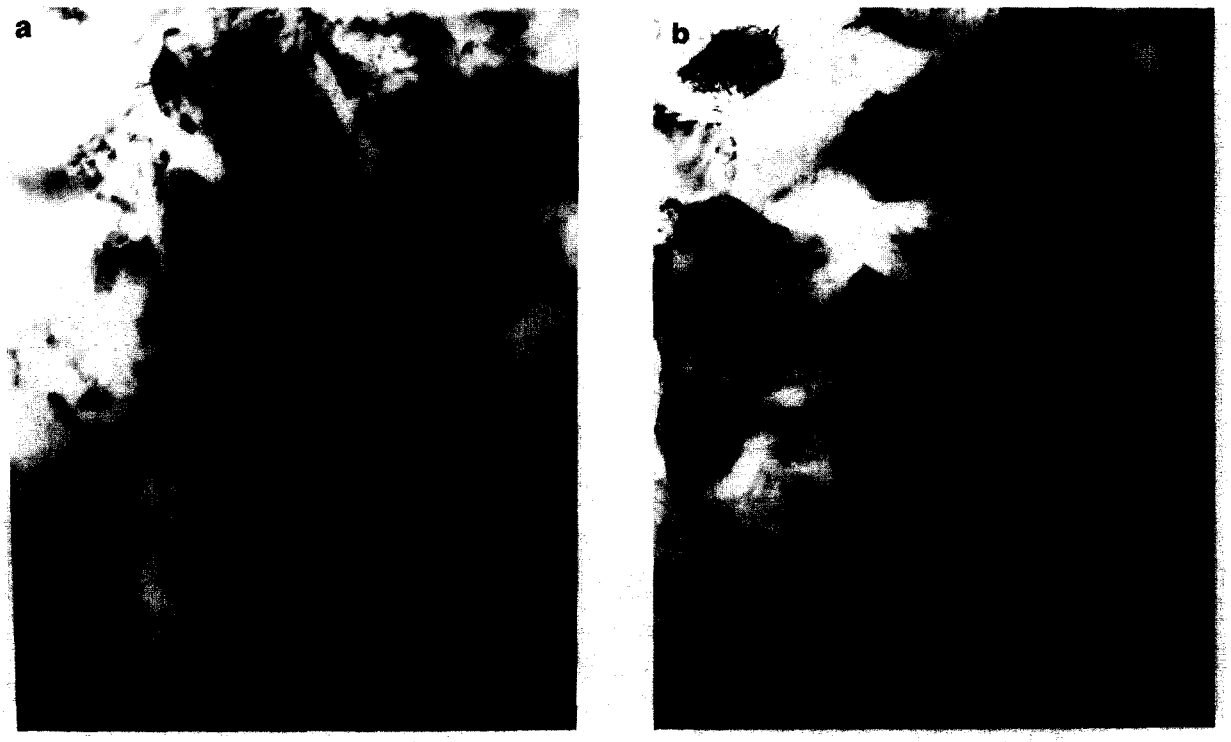

Fig. 14. (a, b) TEMs of specimen D (shear displacement of 0.46 mm); elongated sub-grains breaking up into equiaxed micro-grains.

Fig. 15. TEM of specimen D (shear displacement of 0.46 mm); equiaxed micro-grains.

specimens in actual experiments will retard instability. The thermal softening parameter, λ, was obtained experimentally.

3.4. Instability and localization

Bai (1990), Clifton (1981), Marchand and Duffy (1988), Wright and Batra (1985), Wright and Walter (1987), and Wright (1990) discussed the onset of localization and recognized that instability in the stress–strain curve precedes it. Homogeneous plastic deformation can take place after $d\sigma/d\epsilon = 0$. A perturbation in stress, strain, or temperature was used to trigger localization. The amplitude of the defect in the perturbation analysis determined the onset of the localization. The findings of this investigation confirm these predictions: whereas instability can set in at a fairly low strain (0.2–0.45) and temperature ($\Delta T \sim 100$–330 K), true localization with the formation of a narrow, well defined shear band requires strain (locally) and temperature that are much higher. The experimental results on hat-shaped specimens shown in Figs. 4 and 5 show that localization (shear-band formation) sets in at a shear strain $\gamma \simeq 2$. This shear strain can be converted into a longitudinal strain and it is equal to 0.83. This is much larger than the instability strain displayed by the low strain-rate curves. Locally, at the shear-band initiation sites, the strain is considerably higher than 0.83, because of the presence of a sharp notch. Dynamic recrystallization requires a temperature of $\sim 0.4T_m$: 776 K. It is proposed that localization is initiated in regions in which the temperature reaches a level of 776 K. The temperature rise associated with the onset of shear-band formation can be estimated from Fig. 4, by converting the plastic energy into a thermal energy. This is an approximate procedure, and two areas are indicated in Fig. 4; they represent lower and upper bounds, and conversion into temperatures, by use of Eq. (5), yields values of 540 and 650 K. The application of the constitutive equation (Eq. (6)) at 10^4 s^{-1} yields a pre-

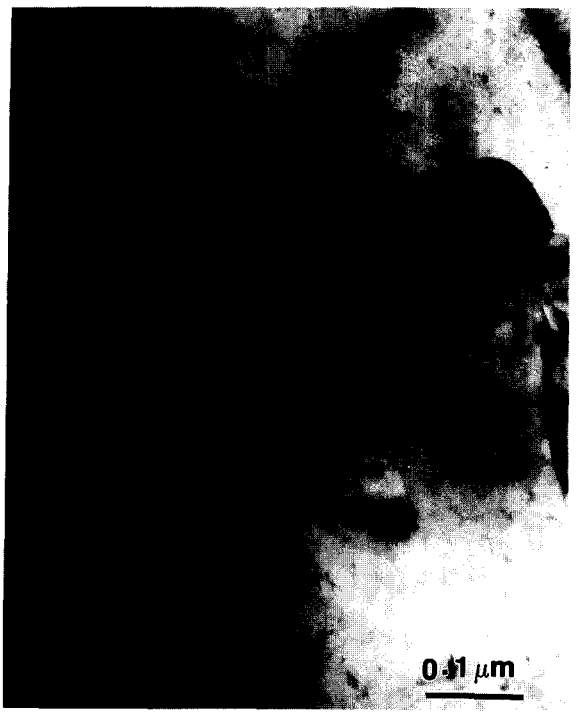

Fig. 16. TEM of specimen D (shear displacement of 0.46 mm); equiaxed micro-grains with low dislocation density.

dicted temperature of 600 K for a strain, $\epsilon = 0.83$. These values are consistent, albeit somewhat lower than the recrystallization temperature (776–970 K). Sharp notches and microstructural inhomogeneities can generate local regions where the plastic strain is considerably higher, and where those temperatures are achieved. At the imposed displacement, d, of 0.41 mm, a strain $\gamma \simeq 1.6$ is created at the notch of the hat by the imposed strain $\epsilon \simeq 0.82$, initiating localization in that area. Subsequently, the localization propagates with a well defined tip as proposed by Kuriyama and Meyers (1986) and Curran and Seaman (1986).

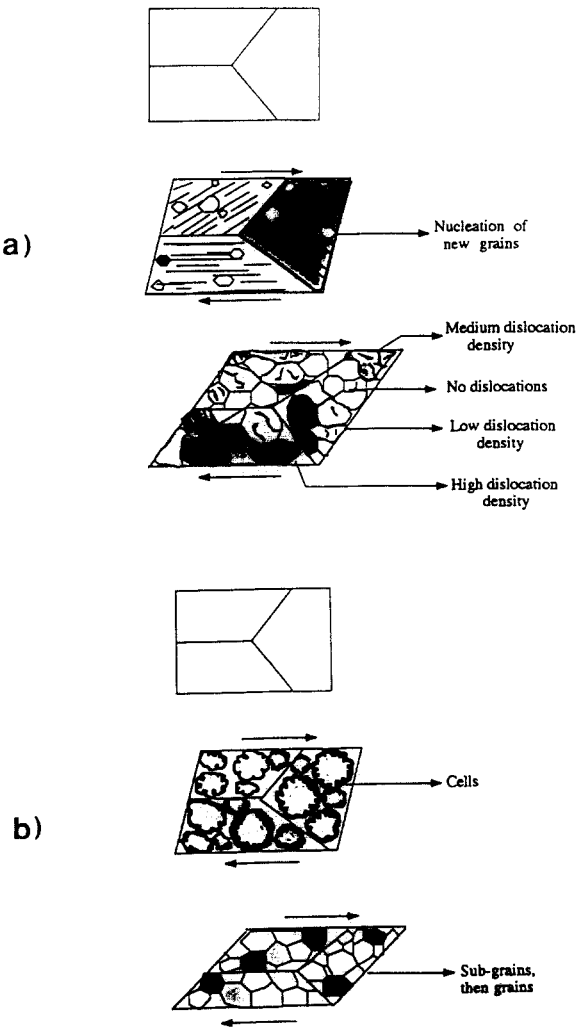

Fig. 17. Schematic representation of: (a) migration; and (b) rotation recrystallization.

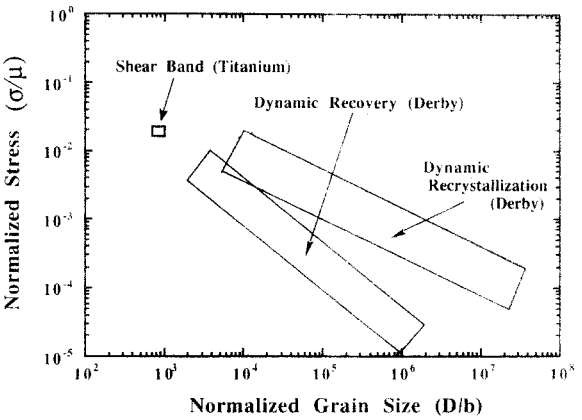

Fig. 18. "Universal" plot of normalized grain size as a function of normalized uniaxial normal stress for dynamic recovery and recrystallization (from Derby (1991)) and titanium datum point.

The mechanism of softening within the shear band is one of dynamic recovery/recrystallization leading to a discontinuity in the flow stress which results in clearly defined boundaries between the shear band and surrounding material. Instability, on the other hand, is the result of softening whereby the short-range component of the dislocation stress is assisted by the thermal energy provided by the temperature rise.

The initiation of localization is a poorly understood phenomenon. Since the scale of localization is so small (thickness of bands is 3–15 μm), this localization is initiated within one single grain and propagates as proposed by Kuriyama and Meyers (1986) and Curran and Seaman (1986). Several possible initiation mechanisms are shown schematically in Fig. 21. They have been classified into geometrical and microstructural. External, geometrical sites are easy to envisage, since they are regions where the concentration of strain leads to a temperature rise with thermal softening. The extremities of the softened region are subjected to a stress concentration which, in turn, leads to a strain concentration and the propagation of the band (Figs. 21a and 21b). Internal, microstructural initiation sites operate in the same manner. Several internal sources of strain con-

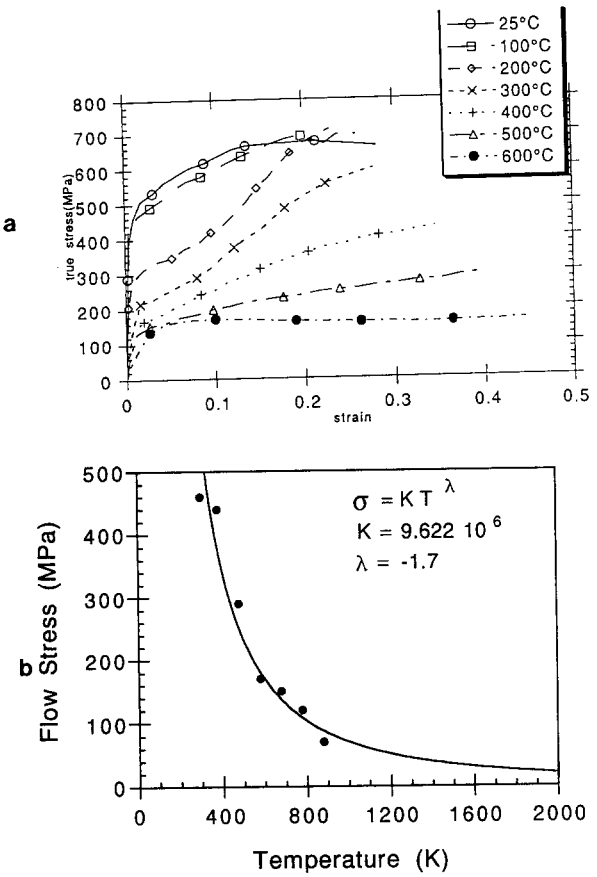

Fig. 19. (a) Stress–strain curves as a function of temperature; (b) flow stress (at plastic strain of 0.1) versus temperature and power-law fit.

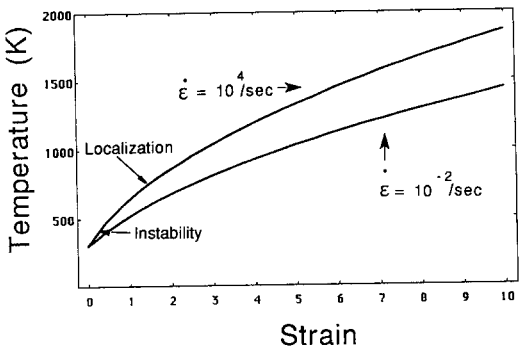

Fig. 20. Temperature rise as a function of plastic strain for two strain rates (10^{-2} and 10^{4} s^{-1}) predicted from constitutive equation; instability and localization temperatures marked.

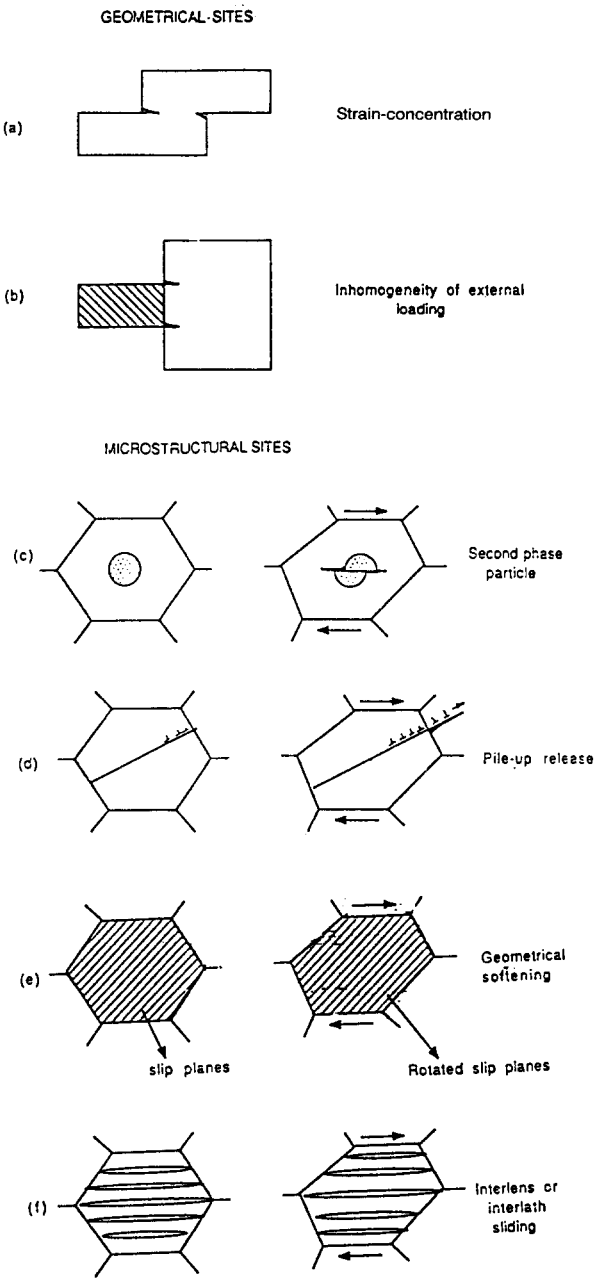

Fig. 21. Geometrical and microstructural initiation sites for adiabatic shear bands.

centration and/or softening are shown in a schematic fashion. If a grain contains a fractured second-phase particle, strain concentration occurs at the extremities of fracture in the matrix,

by virtue of sliding of the fractured interfaces, Fig. 21c. Dislocation pile-ups can, upon their release, pierce a grain, generating localized heating, Fig. 21d. This was initially proposed by Armstrong et al. (1982). If a crystal is favorably oriented for rotational softening, its Schmid factor will decrease with plastic strain, decreasing its "effective" flow stress. This leads, in turn, to a concentration of strain in this grain, Fig. 21e. Martensitic lenses or laths are crystallographically oriented within each grain, and inter-lath or inter-lens sliding is a favored deformation mechanism because the retained austenite has a lower flow stress than the transformed region. Thus, there will be a tendency for the lenses or laths to orient themselves with the shear direction; the same happens in mechanical twinning. This can lead to localized heating, with shear band initiation, Fig. 21f. For the geometry used in the current experiments, the initiation of localization is most probably triggered by geometrical sites, like the stress raisers at the ends of hat-shaped specimens.

4. Conclusions

Mechanical tests conducted on cylindrical specimens over a wide range of strain rates (2×10^{-4} s^{-1} to 7.6×10^{3} s^{-1}) were used to obtain the parameters in a phenomenological constitutive equation (Johnson–Cook). The instability strain and temperature were obtained from the equation by setting $d\sigma/d\epsilon = 0$. These values are consistent with the observed maximum in the stress–strain curve observed at 1 s^{-1} at $\epsilon \simeq 0.45$. High strain-rate experiments conducted on hat-shaped specimens leading to high strains in a narrow shear deformation region yielded adiabatic shear bands when the imposed strain exceeded $\epsilon \simeq 0.83$. Microstructural observations by transmission electron microscopy revealed that the shear-band region consisted of a mixture of equiaxed micrograins (~ 0.2 μm) and elongated subgrains, in contrast with the initial microstructure, which exhibited a grain size of ~ 72 μm. The experimental results indicate that instability is the result of a gradual softening produced by heating, whereas localization is produced by dynamic recovery/recrystallization, leading to a flow stress discontinuity which ensures a clear boundary between the shear band and surrounding material. The size of the micrograins observed in the shear band is consistent with predictions based on dynamic recovery/recrystallization theories.

Acknowledgements

This research was supported by the National Science Foundation under grant No. MSS-9021671 and by the U.S. Army Research Office. Discussions with Professor Y. Bai (Institute of Mechanics), Mr. J. Isaacs, Professor S. Nemat-Nasser, Professor G. Ravichandran (California Institute of Technology), and Professor K.S. Vecchio are gratefully acknowledged. Mr. G. Immaneni, Mr. D. Sil, Mr. S. Lichtenberger, and Dr. U. Andrade provided valuable help at different stages of this investigation and their contribution is greatly appreciated. Split Hopkinson pressure bar experiments and quasi-static experiments on MTS were performed at the Graduate Aeronautical Laboratories, California Institute of Technology, Pasadena. The authors acknowledge Professor G. Ravichandran for the use of these facilities.

References

Armstrong, R.W., C.S. Coffey and W.L. Elban (1982), Adiabatic heating at a dislocation pile-up avalanche, *Acta Metall. 30*, 2111.

Bai Y.L. (1981), A criterion for thermo-plastic shear instability, in: M.A. Meyers and L.E. Murr, eds., *Shock Waves and High-Strain-Rate Phenomena in Metals*, Plenum, New York, p. 277.

Bai, Y.L. (1990), Adiabatic shear banding, *Res Mech. 31*, 133.

Bai, Y.L., C.M. Cheng, and Y.-S. Ding, 1987, Development of thermoplastic shear bands in simple shear, *Res Mechanica, 22*, 1987.

Bai, Y.L., C. Cheng and S. Yu (1986), Width of adiabatic shear bands, *Acta Mech. Sinica 2*, 1.

Beatty, J.H., L.W. Meyer, M.A. Meyers and S. Nemat-Nasser (1992), Formation of controlled adiabatic shear bands in AISI 4340 high strength steel, in: M.A. Meyers, L.E. Murr and K.P. Staudhammer, eds., *Shock Waves and High-*

Strain-Rate Phenomena in Materials, Marcel Dekker, New York, p. 645.

Bird, J.E., A.K. Mukherjee and J.F. Dorn (1969), Correlations between high-temperature creep behavior and structure, in: D.G. Brandon and A. Rosen, eds., *Quantitative Relation Between Properties and Microstructure*, Israel Universities Press, Jerusalem, p. 255.

Carslaw, H.S. and J.C. Jaeger (1959), *Conduction of Heat in Solids*, Oxford U. Press, London, p. 131.

Clifton, R.J. (1981), in: W. Herrmann, ed., *Material Response to Ultra High Loading Rates*, NMAB, NMAB-356, National Academy of Sciences, Washington, p. 129.

Culver, R.S. (1973), Thermal instability in dynamic plastic deformation, in: R.W. Rohde, B.M. Butcher, J.R. Holland and C.H. Karnes, eds., *Metallurgical Effects at High Strain Rates*, Plenum, New York, p. 519.

Curran, D. and L. Seaman (1986), Computational models for nucleation, growth, and coalescence of adiabatic shear bands, in: Y.M. Gupta, ed., *Shock Waves in Condensed Matter*, Plenum, New York, p. 315.

Derby, B. (1992), The dependence of grain size on stress during dynamic recrystallization, *Acta Metall. 39*, 955.

Derby, B. and M.F. Ashby (1987), On dynamic recrystallization, *Scripta Metall. 21*, 879.

Dodd, B. and Y. Bai (1989) Width of adiabatic shear bands found under combined stress, *Mater. Sci. Technol 5*, 557.

Follansbee, P.S. and U.F. Kocks (1988), A constitutive description of the deformation of copper based on the use of the mechanical threshold stress as an internal state variable, *Acta Metall. 36*, 81.

Fressengeas, C. and A. Molinari (1987), Instability and localization of plastic flow in shear at high strain rates, *J. Mech. Phys. Solids 35*, 185.

Grebe, H.A., H.-r. Pak and M.A. Meyers (1985), Adiabatic shear localization in titanium and Ti-6 pct Al-4 pct V alloy, *Metall. Trans. A 16A*, 761.

Hartley, K.A. J. Duffy and R.H. Hawley (1987), Measurement of the temperature profile during shear band formation in steels deforming at high strain rates, *J. Mech. Phys. Solids 35*, 283.

Hartmann, K.-H., H.-D. Kunze and L.W. Meyer (1981), Metallurgical effects on impact loaded materials, in: M.A. Meyers and L.E. Murr, eds., *Shock-Wave and High-Strain-Rate Phenomena in Materials*, Marcel Dekker, New York, p. 325.

Klepaczo, J.R. (1988), Constitutive modeling in dynamic plasticity based on physical state variables – A review, *J. de Physique 49, Suppl. 9*, C3–553.

Kuriyama, S. and M.A. Meyers (1986), Numerical modeling of the tip of an adiabatic shear band, *Metall. Trans. 17A*, 443.

Johnson, G.R. and W.H. Cook (1983), A constitutive model and data for metals subjected to large strains, high strain rates, and high temperatures, *Proc. 7th Int. Symp. on Ballistics*, The Hague, Netherlands.

Marchand, A. and J. Duffy (1988), An experimental study of the formation process of adiabatic shear bands in a structural steel, *J. Mech. Phys. Solids 36*, 251.

Meyer, L.W. and S. Manwarig (1986), Critical adiabatic shear strength of low alloyed steel under compressive loading, in: L.E. Murr, K.P. Staudhammer and M.A. Meyers, eds., *Metallurgical Application of Shock-Wave and High-Strain-Rate Phenomena*, Marcel Dekker, New York, p. 657.

Meyers, M.A. and H.-r. Pak (1986), Observation of an adiabatic shear band in titanium by high-voltage transmission electron microscopy, *Acta Metall. 34*, 2493.

Meyers, M.A., L.W. Meyer, J. Beatty, U. Andrade, K.S. Vecchio and A.H. Chokshi (1992), High strain, high strain-rate deformation of copper, in: M.A. Meyers, L.E. Murr and K.P. Staudhammer, eds., *Shock Waves and High-Strain-Rate Phenomena in Materials*, Marcel Dekker, New York, p. 529.

Moss, G. L. (1981), Shear strain, strain rates, and temperature changes in adiabatic shear bands, in: M.A. Meyers and L. E. Murr, eds., *Shock Waves and High-Strain Rate Phenomena in Metals,* Plenum, New York, p. 299.

Recht, R.F. (1964), Catastrophic thermoplastic shear, *J. Appl. Mech. 31*, 189.

Sandstrom, R. and R. Lagneborg (1975), A model for static recrystallization after hot deformation, *Acta Metall. 23*, 481.

Stelly, M. and R. Dormeval (1986), Adiabatic shearing, in: M.A. Meyers, L.E. Murr and K.P. Staudhammer, eds., *Metallurgical Applications of Shock-Wave and High-Strain-Rate Phenomena*, Marcel Dekker, New York, p. 607.

Timothy, S.P. and I.M. Hutchings (1985) The structure of adiabatic shear bands in a titanium alloy, *Acta Metall. 33*, 667.

Timothy, S.P. (1987), The structure of adiabatic shear bands in metals: A critical review, *Acta Metall. 35* 301.

Winter, R.E. (1975), Adiabatic shear in titanium and polymethylmethacrylate, *Philos. Mag. 31*, 765.

Wright, T.W. (1990), Approximate analysis for the formation of adiabatic shear bands, *J. Mech. Phys. Solids 38*, 515.

Wright, T.W. and J.W. Walter, (1987), On stress collapse in adiabatic shear bands, *J. Mech. Phys. Solids 35*, 701.

Wright, T.W. and R.C. Batra (1985) The initiation and growth of adiabatic shear bands, *Int. J. Plast. 1*, 205.

Zerilli, F.J. and R.W. Armstrong (1987) Dislocation-mechanics-based constitutive relations for material dynamics calculations, *J. Appl. Phys. 61*, 1816.